Electronic Supplementary Material (ESI) for Lab on a Chip.
This journal is © The Royal Society of Chemistry 2017
Electronic Supplementary Material (ESI) for Lab on a Chip.
This journal is ©The Royal Society of Chemistry 2017

Supporting Information

Controlled rotation and translation of spherical particles or living cells by Surface Acoustic Waves.

Ianis Bernard,[a] Alexander A. Doinikov,[a] Philippe Marmottant,[a] David Rabaud,[b] Cédric Poulain[b] and Pierre Thibault[a]

[a] CNRS / Université Grenoble-Alpes, LIPhy UMR 5588, Grenoble, F-38401, France.

[b] Univ. Grenoble Alpes, CEA, LETI MINATEC Campus, F-38000 Grenoble, France.

Corresponding author:

E-mail: Pierre.Thibault@univ-grenoble-alpes.fr. Tel: +33 (0)668 104 915. Fax: +33 (0)476 635 495.

1. Simple model taking into account reflections between electrodes

In order to get the pressure field from two counter propagating waves, we can consider two sources located at positions $\pm d$ from the center, and say along $\mathbf{e}_\mathrm{x}$. If in addition we impose some phase lags $\phi_x^\downarrow$ and $\phi_x^\uparrow$ for each source, the total pressure field along this axis is

$$\underline{p}_\mathrm{in}(x,t) = \frac{p_{0x}}{2}\exp\left(-i\omega t\right)\left[\exp\left(i(k_\mathrm{x}(x+d) - \frac{\pi}{2} + \phi_x^\downarrow)\right) + \exp\left(i(-k_\mathrm{x}(x-d) + \frac{\pi}{2} + \phi_x^\uparrow)\right)\right] \tag{S1}$$

Assuming the distance between the IDTs is an integer number ($2d = n\lambda_\mathrm{x}$), we get

$$\underline{p}_\mathrm{in}(x,t) = p_{0x}\exp\left(-i\left(\omega t - \frac{(\phi_x^\downarrow + \phi_x^\uparrow)}{2}\right)\right)\sin\left(k_\mathrm{x}x + \frac{\phi_x^\downarrow - \phi_x^\uparrow}{2}\right) \tag{S2}$$

which clearly shows how to implement a phase lag and at what position. While this expression

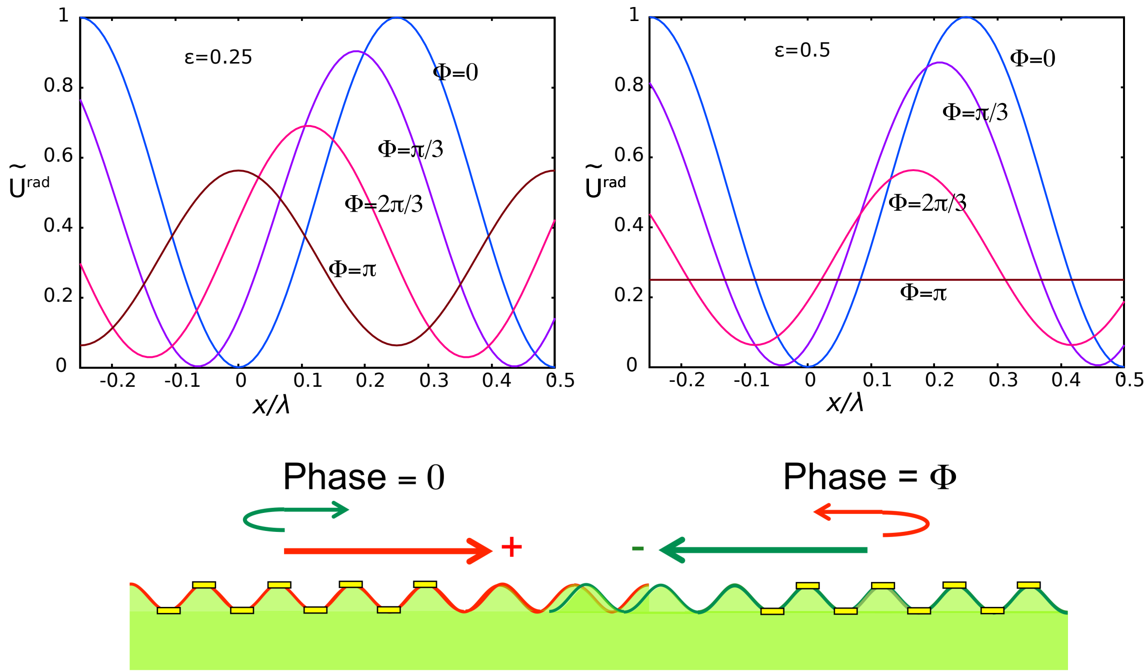

Figure S1. Upper curves: Reduced Gor'kov's acoustic potential $U^{\mathrm{rad}}(x)$ along x-direction for reflection coefficients $\varepsilon = 0.25$ and $\varepsilon = 0.5$. The different curves correspond to different values of ϕ and potential minima to acoustic traps. Lower scheme: superimposition of two counter propagating waves with different amplitudes due to a phase lag φ, including some partial mechanical reflection between electrodes.

assumes that the amplitude of the standing wave is that of individual sources, it ignores reflections that can occur between emitters and that exist if all the energy emitted by the sources is not radiated in the liquid, in which case we would also have to consider the decay to the wave along its path, another important phenomenon. To illustrate this phenomenon, let $\phi_x^\uparrow$ be the reference phase ($\phi_x^\uparrow = 0$) and write $\phi_x^\downarrow = \phi$. If one assumes that the reflection between electrodes leads to part of the wave with a phase that is imposed by the distance between electrodes and part of the wave with an phase that can be tuned in a ratio ε, we get for the normalized pressure $\tilde{p}_{\text{in}} = p_{\text{in}}(x,t)/p_{0x}$:

$$\tilde{p}_{\text{in}}(x,t) = \varepsilon \cos(\omega t)\sin(k_{\text{x}}x) + (1-\varepsilon)\cos(\omega t - \phi/2)\sin(k_{\text{x}}x + \phi/2) \tag{S3}$$

Correspondingly, the normalized Gor'kov potential along the x-direction becomes:

$$\tilde{U}^{\text{rad}}(x) = \varepsilon^2 \sin(2k_{\text{x}}x) + (1-\varepsilon)^2 \sin^2\left(k_{\text{x}}x + \frac{\phi}{2}\right) + 2\varepsilon(1-\varepsilon)\sin(k_{\text{x}}x)\sin\left(k_{\text{x}}x + \frac{\phi}{2}\right)\cos\left(\frac{\phi}{2}\right) \tag{S4}$$

This potential is plotted in Fig. S1 for the two cases $\varepsilon = 0.25$ and $\varepsilon = 0.5$. While for ideal sources the particles are free to move whatever the phase ϕ is, the potential minima where the particles are trapped depend on the applied phase in practice ($\varepsilon \neq 0$). As a consequence, the particles may no longer follow the acoustic potential drift but instead stay at a same location. Movie S8 illustrates this situation in the case $\varepsilon = 0.4$. In the presence of an external flow, for instance due to acoustic streaming developing in the whole acoustic chamber, the particles will be preferentially dragged in the flow direction, and one loses control of their positions. Accordingly, their rotation speeds may differ from the expected values. These are yet major experimental limitations encountered in the experiments, that we overcome by minimizing reflections between electrodes, matching their mechanical impedances with the surrounding environment.

2. 3D model for radiation forces

While the calculation of the acoustic potential given in eqn (11) is valid close enough from the emitting surface, it is clear from Fig. 2 (see main text) that the actual acoustic potential is more complex due to the reflection of the acoustic field on the upper rigid wall. As a consequence, the acoustic potential is due both to waves emitted into the liquid along direction k_f^+ and k_f^- but also to reflections on the upper wall. In addition, the displacement $\underline{\xi}_s(x,y,t)$ associated to the surface wave is not as simple as that previously considered, due to the elliptical motion of the points at the surface in the $x-z$ and $y-z$ planes: the propagation of a wave along $\mathbf{e}_{\text{x}}$ or $\mathbf{e}_{\text{y}}$ causes a displacement along $\mathbf{e}_{\text{z}}$, and also along the propagation direction. For $LiNbO_3$, considering for simplicity that the crystal is isotropic, the ratio of amplitudes is approximately[1]:

$$\varsigma = \xi_{0y}^y/\xi_{0z}^y = \xi_{0x}^x/\xi_{0z}^x \approx 0.6 \tag{S5}$$

For two ideal orthogonal standing waves with a phase lag φ, the vibration of the crystal thus becomes

$$\underline{\xi}_s(x,y,t) = e^{i(\omega t + \pi/2)} \begin{pmatrix} \varsigma \xi_{0z}^x \sin(kx) \\ \varsigma \xi_{0z}^y \sin(ky) e^{i\varphi} \\ \xi_{0z}^x \cos(kx) + \xi_{0z}^y \cos(ky) e^{i\varphi} \end{pmatrix} \tag{S6}$$

(Note that we use here a sine function for the displacement and therefore a cosine function for the pressure field in eqn (27), in consistency with Fig. 10 and Fig. 15 of the simulated acoustic potentials.) We recognize in expression (S6) the first two components responsible for the swirling motion of the surface plus an additional vertical component. Using the work by Haake[2], it can be shown that the velocity potential in the whole volume can be expressed as

$$\underline{\psi}_1 = \frac{i\omega}{k_{fz}\sin(k_{fz}h)} \underline{\xi}_s(x,y,t)\cos(k_{fz}(h-z)) \tag{S7}$$

It is easy to check that the form of $\underline{\psi}_1$ gives the correct boundary conditions, since from $\underline{\xi}_1 = \frac{1}{i\omega}\nabla\underline{\psi}_1$ we get for the vertical component of the displacement

$$\underline{\xi}_{1z} = \frac{1}{\sin(k_{fz}h)}\underline{\xi}_{sz}(x,y,t)\sin(k_{fz}(h-z)) \tag{S8}$$

which gives $\underline{\xi}_{1z} = \underline{\xi}_{sz}$ for $z=0$ and $\underline{\xi}_{1z} = 0$ for $z=h$. In the case the anisotropy of the crystal is neglected, the $x-y$ in plane component responsible for the rotation can thus be factorized and separated from the vertical component. When taking into account the anisotropy, the levitation levels due to the two orthogonal waves being slightly different, a slow additional out-of plane rotation is expected, observable in experiments on spherical objects. It is interesting to notice the discontinuity of $\underline{\xi}_{1x}$ and $\underline{\xi}_{1y}$ in view of the hypothesis of an inviscid fluid. Furthermore, the amplitude diverges for a channel height h being a multiple of λ_{fz} since the model assumes a continuous injection of acoustic energy which is not compensated by losses. Using the definition of the Rayleigh angle (see Fig. 2) and calling $\chi = k_s/k_{fz} = \tan(\theta_R) \approx 0.4$, we can get the first order velocity field:

$$\underline{\mathbf{v}}_1 = \frac{\omega}{\sin(k_{fz}h)}e^{i\omega t}\begin{pmatrix} \xi_{0z}^x\chi\sin(kx)\cos(k_{fz}(h-z)) \\ \xi_{0z}^y\chi\sin(ky)\cos(k_{fz}(h-z))e^{i\varphi} \\ \left(\xi_{0z}^x\cos(kx)+\xi_{0z}^y\cos(ky)e^{i\varphi}\right)\sin(k_{fz}(h-z)) \end{pmatrix} \tag{S9}$$

and from Euler's equation we deduce for the first order pressure field

$$\underline{p}_1 = i\frac{\rho_0\omega^2}{k_{fz}\sin(k_{fz}h)}e^{i\omega t}\left[\xi_{0z}^x\cos(kx)+\xi_{0z}^y\cos(ky)\,e^{i\varphi}\right]\cos(k_{fz}(h-z)) \tag{S10}$$

According to Gor'kov, we can compute the acoustic potential from the first order quantities, by evaluating the sum of the time averaged potential and kinetic energies, which are:

$$\langle e_{p2}\rangle = \frac{\underline{p}_1\,\underline{p}_1*}{4\rho_0 c_0^2} = \frac{k_{fz}^2\left(1+\chi^2\right)}{4\rho_0\omega^2}\underline{p}_1\,\underline{p}_1* \tag{S11}$$

and

$$\langle e_{c2}\rangle = \frac{1}{4}\rho_0\underline{\mathbf{v}}_1\cdot\underline{\mathbf{v}}_1* \tag{S12}$$

where we have used

$$k_f = \sqrt{k_{fz}^2+k_s^2} = k_{fz}\sqrt{1+\chi^2} = \omega/c_0 \tag{S13}$$

The total acoustic potential thus writes:

$$\begin{aligned} U^{\mathrm{rad}} =& \frac{V_p}{4}\rho_0\left(\frac{\omega}{\sin(k_{fz}h)}\right)^2\Big\{\left[{\xi_{0z}^x}^2\cos^2(kx)+{\xi_{0z}^y}^2\cos^2(ky)\right]\times\left(\left[f_1\left(1+\chi^2\right)+\tfrac{3}{2}f_2\right]\cos^2(k_{fz}(h-z))-\tfrac{3}{2}f_2\right) \\ &-\tfrac{3}{2}f_2\chi^2\left({\xi_{0z}^x}^2\sin^2(kx)+{\xi_{0z}^y}^2\sin^2(ky)\right)\cos^2(k_{fz}(h-z)) \\ &+\xi_{0z}^x\xi_{0z}^y\cos(kx)\cos(ky)\cos(\varphi)\times\left(2f_1\left(1+\chi^2\right)\cos^2(k_{fz}(h-z))-3f_2\sin^2(k_{fz}(h-z))\right)\Big\} \end{aligned} \tag{S14}$$

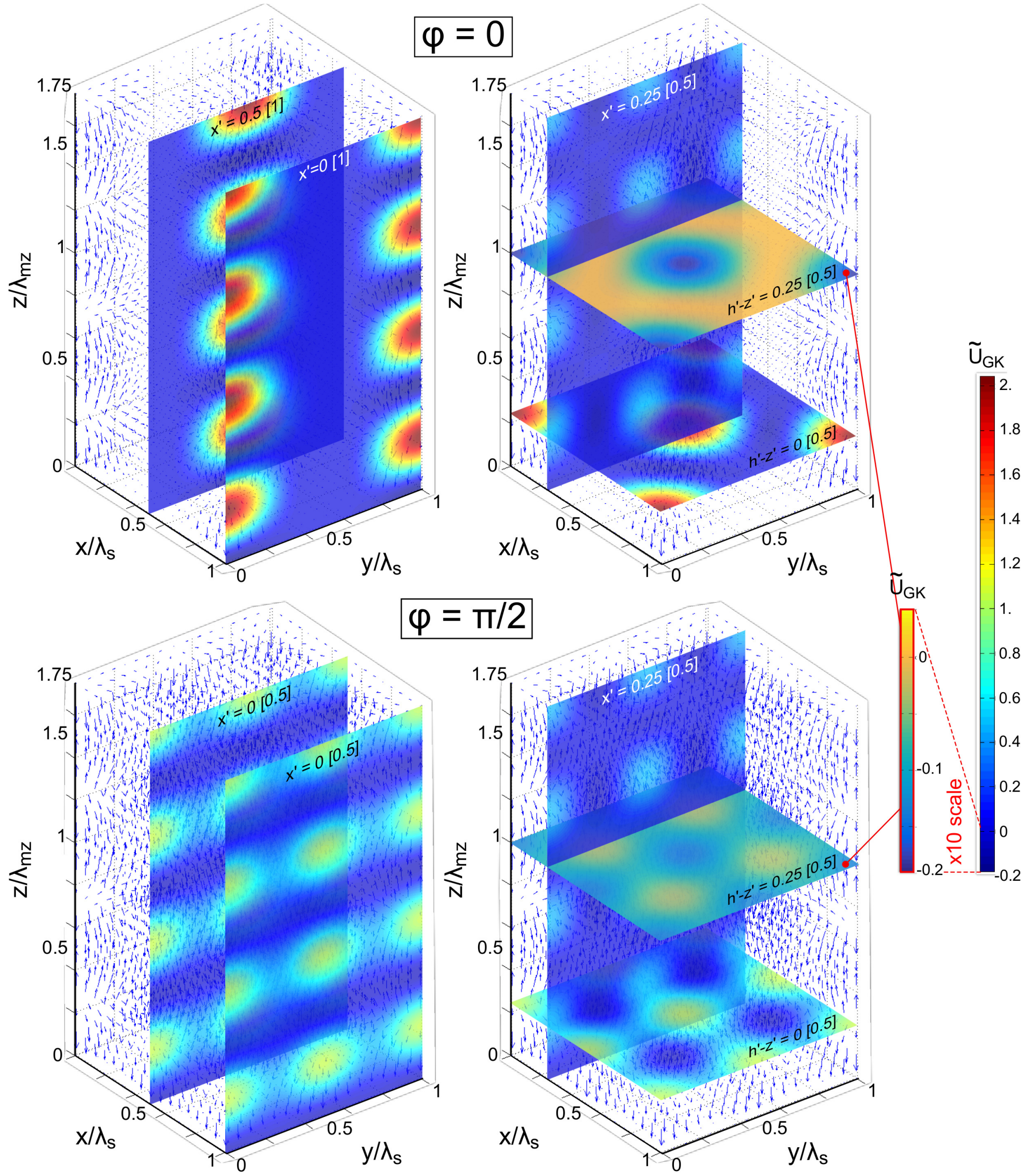

Figure S2. Normalized acoustic potential and forces computed for PS beads in water (for two orthogonal acoustic waves of equal amplitude ($\xi_{0z}^{x}=\xi_{0z}^{y}$) for the two phase lags $\varphi=0$ and $\varphi=\pi/2$. For the computation, $h=1.75\lambda_{fz}$. In levitation planes corresponding to $(h-z)/\lambda_{fz}=0\,[1/2]$, the gradients are particularly weak and the contrast has been enhanced by ten times.

This normalized potential $\tilde{U}^{\mathrm{rad}}=4\rho_0\left(\dfrac{\omega}{\sin(k_{fz}h)}\right)^{-2}\dfrac{U^{\mathrm{rad}}}{V_p}$ and the corresponding force have been represented in Fig. S2 for PS beads in water, in the case $\xi_{0z}^{x}=\xi_{0z}^{y}$. At a height of z/λ_{fz}=0 [1/2], the 2D acoustic potential shown in Fig. 6a and 6b is recovered, which corresponds to the absolute minima of the potential. Due to the presence of a standing wave in the vertical direction, some levitations planes are also created, at heights z/λ_{fz}=1/4 [1/2], with a much lower in plane modulation of the acoustic potential but strong vertical compression. Note that in this 3D model, the hypothesis of small beads respective to the wavelength is not fully justified, since $k_f a$ is not negligible compared to 1.

3. Movies

Supplementary movie S1 Numerical simulation of the motion at the surface of a the piezo substrate due to two orthogonal standing surface acoustic waves. The lateral dimensions of the domain are one wavelength and the phase lag between the two orthogonal directions x and y is $\varphi = \pi/2$. The black vectors are the in-plane projection of the vectors normal to the wave-front. The direction of rotation of the surface alternates every half-wavelength.

Supplementary movie S2 Rotation of a single Janus bead, 10 μm in diameter suspended in a microfluidic channel (slow motion $/10$).

Supplementary movie S3 Rotation of multiplets. Depending on its symmetry, a multiplet can either rotate like a single entity, of like on object that can be trapped in the acoustic field. Thus, associations of 2, 4, etc. particles tend to align along the acoustic potential, whereas single particles or groups of 3 or 5 beads are free to rotate.

Supplementary movie S4 Rotation of a white blood cell (WBC) and of a red blood cells (RBC) suspended in a microfluidic channel. The larger WBC rotates clockwise while a smaller RBC is seen to rotate anti clockwise when sound is turned on. In the absence of a reflector, the suspended particles may eventually stop their rotation due to the proximity of the channel wall.

Supplementary movie S5 Observation of the rotation of RBC diluted in PBS due to two orthogonal acoustic waves of a same frequency of 37.1 MHz and with a varying phase lag φ between 0° and 360° by steps of 15° every 5s.

Supplementary movie S6 Experimental record of the combined drift and rotation of a Janus sphere.

Supplementary movie S7 Numerical simulation of the combined drift and rotation of a Janus sphere (see main text).

Supplementary movie S8 Numerical simulation of the displacement of a particle as a function of the relative phase lag between two opposite IDTs assuming a finite reflection coefficient $\varepsilon = 0.4$.

References

1 N. Nama, R. Barnkob, Z. Mao, C. J. Kähler, F. Costanzo and T. J. Huang, Lab on a Chip, 2015, **15**, 2700–2709.
2 A. Haake, Ph.D. thesis, Swiss Federal Institute of Technology Zurich, 2004 - 149 pages (see model page 44 and following).